JOURNAL OF CATALYSIS 7, 179–190 (1967)

Diffusional Mass Transport of Nonadsorbed Gases within Porous Structures

I. Experimentation and Correlation

RICHARD N. FOSTER,* JOHN B. BUTT, AND HARDING BLISS

From the Department of Engineering and Applied Science, Yale University New Haven, Connecticut

Received August 24, 1966; revised October 24, 1966

Counterdiffusion flux and flux ratio have been measured for the argon-helium system in four different, well-characterized porous structures. Pressures from 1 to 14.6 atm and temperatures from 0° to 69°C were employed in the investigation. Care was taken to avoid the effects of extraneous factors in experimental work, and to ensure the absence of transport by surface diffusion. Variation of flux with pressure, temperature, and porosity is discussed with regard to the equations defining diffusion in transition range capillaries.

The mechanism of mass transport within a porous solid is an extremely complex one which is very much dependent on the nature of the porous structure involved. Obvious importance in reaction processes employing supported catalytic materials (*1*, *2*) has prompted considerable work on the problem (*3*), most often by incorporating structural effects on mass transport into an effective diffusivity which then is employed as a parameter in the solution of the normal diffusion equation. Effective diffusivity values are notoriously specific, often useful for empirical representation but rarely for prediction of structural influence on rates of diffusion. Numerous attempts have been made to show explicitly the relationship between porous structure and effective diffusivity, commencing with analysis in terms of tortuosity or labyrinth factor and more recently through postulation of detailed structural models (*4*, *5*, *6*).

The development of a theory for diffusion in transition capillaries (*7*, *8*) where the diameter is of the same order as molecular mean free paths, has provided a sound basis for discarding the overall approach. Pore structure effects are analyzed by consideration of the transport process in individual pores, with subsequent assembly of this into an appropriate overall description. The transport equation written in terms of mole fraction for one-dimensional diffusion under isothermal, isobaric conditions is

$$N_A = cD_{AB}[(1 - \alpha y) + \gamma]^{-1}\nabla y \qquad (1)$$

where N_A is the flux of component A (moles/time-area), c is total concentration (moles/volume), D_{AB} the bulk diffusion coefficient (area/time), y the mole fraction of A, γ the ratio of D_{AB} to D_K (the Knudsen diffusion coefficient), and α, a flux ratio related quantity which has been shown (*7*, *9*, *10*) to be given by $[1 - (M_A/M_B)^{1/2}]$ for all capillaries and conditions of interest in this work.

We have recently proposed a computational model for pore structure (*11*) in which resistance to diffusion may be determined by means of Eq. (1) on construction of a suitable array of cylindrical pores. The model considers void volume to consist of two major arrays of pores, each

* Present address: Union Carbide International Co., New York, N. Y.

divided into two halves which are mirror images of each other. The two arrays are conical in shape, one narrowest at the center which is termed centrally convergent, and one widest at the center which is called centrally divergent (see Fig. 1).

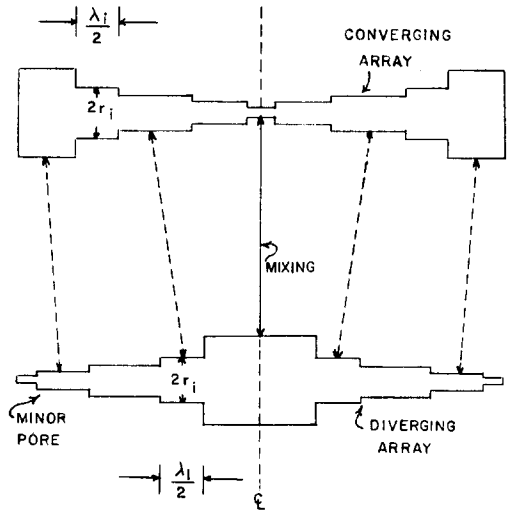

FIG. 1. Simplified geometric representation of the convergent–divergent pore array.

The exact shape of these arrays is determined uniquely by the internal volume–area distribution of the porous structure it is desired to model. Diffusional path lengths are normalized with respect to overall dimensions, so the two-pore combination is computationally equivalent to n centrally convergent and n centrally divergent pore arrays of the same total volume. The concentrations of material diffusing through each of the arrays are functions of the initial concentrations and the geometry of the individual segments (or minor pores) of the arrays. Hence, concentration drop over each segment differs for the centrally convergent and centrally divergent arrays due to the functional dependence of concentration on radius and length expressed by Eq. (1). Simulation of mixing in actual structures is provided by mixing the concentrations at various points within the arrays as specified by a mixing parameter determined by total length agreement between the segments of the two arrays. This is indicated in Fig. 1 by the solid and dotted lines joining the two arrays. The flux–concentration relationship is computed from rearrangement of Eq. (1)

$$y_{i+1} = (1/\alpha)\{[(1 - \alpha y_i) + \gamma_i] \exp [N_A c \lambda_i \alpha / D_{AB}] - (\gamma_i + 1)\} \quad (2)$$

where λ_i is the length of the pore segments corresponding to radius r_i, and y_i and y_{i+1} are mole fractions of diffusing species at the entrance and exit of the minor pore considered. The mixing calculation is carried out according to

$$y_{av} = \frac{y_{CC}\Delta V_{CC} + y_{CD}\Delta V_{CD}}{\Delta V_{CC} + \Delta V_{CD}} \quad (3)$$

where subscripts CC and CD refer to the convergent and divergent arrays, respectively, and ΔV represents the volumes to be mixed at point i within the array (numerically equivalent to the volumes of the two minor pores involved).

This convergent–divergent pore model for porous structure effects accounts in principle for both parallel and series diffusional paths, for mixing and for the multidimensional nature of the transport process. It is also an important characteristic of the model that the geometric properties of the pore arrays are uniquely determined by the volume–area distribution as determined by analysis of adsorption or penetration experiments. A detailed discussion of the model has been given elsewhere (*11*), including a demonstration of its utility in representation of some experimental results on mass transport through porous solids. The amount of reliable experimental data on effective diffusion rates in porous materials from previous experimentation is astonishingly small, however, due both to obscuring effects such as boundary layer diffusion or surface migration or to insufficient characterization of the physical properties of the structures studied. There is considerable need for reliable experimental data on diffusional rates of nonadsorbed gases through porous solids to permit study of the relation between the porous structure and the observed diffusion process. The

methods and objectives of the present work are both experimental and theoretical: to conduct precise experimentation on rates of diffusional transport of nonadsorbed gases through porous materials for which all pertinent characteristics have been determined, to carry out these studies over a wide range of temperature, pressure, and porous structure properties, to interpret the data so obtained in terms of the convergent–divergent pore model, and to relate the interpretation obtained through use of the computational model to the properties of some limiting types of real porous structures.

Experimental

Measurement of Diffusion Rates

A convenient technique for study of transport in porous structures is measurement of the counterdiffusion flux through a plug at constant total pressure and temperature. The best method for accomplishing this is the Weisz (*12*) modification of the Wicke-Kallenbach (*13*) experiment. In this system a single pellet is placed between streams of different gas composition. Normally the system is such that different pure gases are on opposite sides of the pellet; pressure and temperature gradients across the pellet are eliminated and the diffusion fluxes are measured in a well-defined manner. Experiments are carried out at various temperatures and pressures and the data obtained demonstrate the dependence of diffusional transport rates on pressure, temperature, and properties of the porous pellet. In addition, the experiment yields information about the ratio of the counterdiffusing fluxes.

Particular care must be taken in the design of the diffusional cell to be used in a Wicke-Kallenbach experiment in order to avoid boundary layer diffusion effects and stagnant areas at the surface of the plug. Elimination of boundary layer effects follows on passing the gaseous streams across the surface at a rate much greater than the diffusion rate through the plug, and stagnant areas are eliminated if the entire pellet surface is contacted uniformly by the gas stream. Essentials of a cell so designed are shown in Fig. 2(a) and are discussed in detail elsewhere (*14*). The basic part of the cell is a metallic ring which contains the porous pellet to be studied. The pellet is actually formed in the ring and thus leakage around the sides of the pellet is minimized.

The diffusion cell is connected to the main flow system, which is made of ¼-inch standard copper tubing, with ¼-inch Swagelok Quick-Disconnects. A schematic of the flow system is given in Fig. 2(b). The diffusion cell is immersed in either a Precision Oil Bath (Model 62690) controlled with a bimetallic regulator to ±0.1°C, or an ice water bath. Temperature was measured with a standard mercury thermometer graduated in 1°C units. Pressure on each side of the cell is controlled independently by two Apco Model 1A backpressure regulators. These regulators are sufficiently precise to allow equalization of pressure on both sides of the diffusion cell to ±0.2 cm water in the range of 0 to 300 psig. Differential pressure across the cell is measured in a glass manometer provided with liquid traps on each side. Absolute pressure is measured on each side of the cell with two Ashcroft 0–600 psig Bourdon gauges graduated in 5-psig increments.

Flow rates across the surfaces of the pellet are controlled independently on each side of the cell with two Whitey 22RS4 needle valves fitted with micrometer handles, permitting reproducible settings from run to run. Flow rates are measured downstream of the diffusion cell and thermal conductivity cell with soap film meters. Two of these were employed to measure flow rates from 0 to 100 cm^3/min, and a larger unit emlpoyed for flows up to 3000 cm^3/min.

Concentrations of the effluent streams were measured with a Gow-Mac 30S thermal conductivity cell and 20-V (Gow-Mac No. 9999) power supply, with output recorded continuously on a Bausch and Lomb 5-inch strip chart recorder. The flow scheme employed contains only one thermal conductivity cell, with a valving

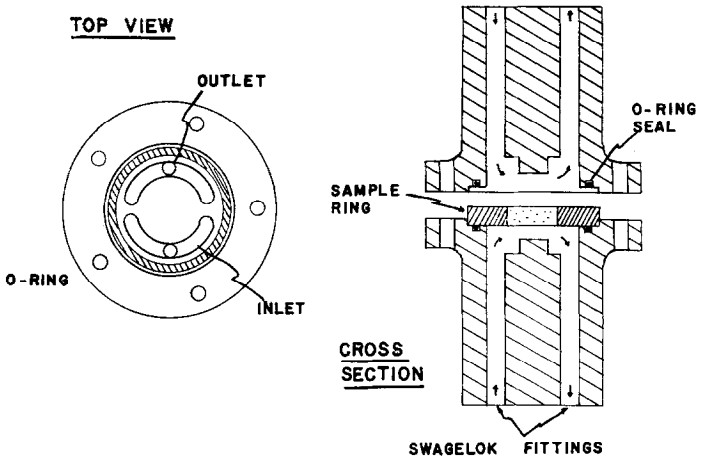

FIG. 2(a). Flow diagram and detail of the diffusion cell.

system downstream of the diffusion cell permitting selection of either effluent stream for measurement, as indicated in Fig. 2(b). The appropriate reference stream for the thermal conductivity cell can also be selected, and provision for bypassing the cell completely with sample gas while simultaneously passing reference gas through each side of the cell is also made in the valving arrangement. With this procedure the base line of the recorder can be checked at any point, regardless of the pressure in the system.

Preparation of Porous Solid Samples

The porous pellets to be studied were made by compressing the basic material, supplied in powder form, into the diffusion cell ring by means of a Carver Model B press. A compression force of 5000 to 12 000 lb was employed, depending on the desired pellet density. After pellet formation, the containing ring was machined to match the surface of the plug and about 0.03 cm was machined off each face of the plug to remove any encrusted surface layer. The homogeniety of the plugs was determined by cutting away portions of the pressed form and weighing the remaining part. The density of the portion removed could then be calculated. Several concentric sections were removed from each layer using larger and larger end mills; in this way pellet density was measured at various positions. Homogeneity tests were carried out on samples prepared from an iron powder, Fe-0303-P, and a nickel oxide supported on kieselguhr.

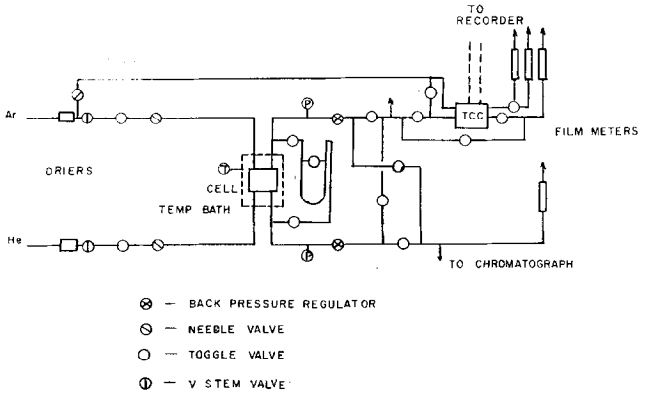

FIG. 2(b). Flow diagram for the Wicke-Kallenbach-type diffusional apparatus.

Ni-0104-P, supplied by the Harshaw Chemical Company. The results of these tests are discussed subsequently. Experimentation on diffusion rates was carried out on the Ni-0104-P and on a molybdena, Mo-0401-P, also supplied by Harshaw.

Experimental Procedure

An experimental run consisted of measuring the diffusional flow of CP grade argon through the porous particle contained within the cell at several pressures and then measuring the flux of CP grade helium at identical pressures. At the start of a run the reference gas was passed on one side of the pellet and through the thermal conductivity cell (TTC) and the second gas passed across the other side of the pellet and through the TCC. The flow rates of all streams were equalized and the differential pressure gauge then opened to the system and the differential pressure across the diffusion cell adjusted to zero. Once the pressure was balanced flows were maintained until steady state, as indicated by invariant flow rates and TCC output, was attained; this procedure normally required about 30 min. At steady state the flow rates were measured and TCC output recorded. Composition of the gas stream was determined from the TCC output by means of a previously determined calibration.

Boundary layer diffusion effects were eliminated by determining the effect of the bulk flow rates of gas past the two pellet faces on the diffusion flux. This was done simply by varying the flow rate and observing the change in apparent diffusion rate. At the point where measured diffusion fluxes became independent of gas flow rates, the operating conditions were noted and maintained throughout the remainder of the run. It is important to recognize the possible strong effects of boundary layer diffusion in this type experiment. It is absolutely necessary to ensure that sufficiently high flow rates past the pellet faces are maintained such that measured diffusional resistances pertain solely to the effects of the porous structure. Difficulties of this sort make questionable much previous data from this type of experiment.

Total pressures within the system were varied by means of the back-pressure regulator adjustment; succeeding pressure levels were ordinarily about 25 psig. above the previous setting and measurements were made up to total pressures of 200 psig. At this point the pressure was released and the same procedure followed for measurements on the other side of the diffusion cell, starting again at atmospheric pressure. Temperature was varied by adjustment of the microregulator setting for the constant temperature bath containing the diffusion cell. Pellets were changed after each complete set of pressure and temperature measurements.

Results

Properties of the Porous Structures

Physical data for the porous solids employed in the experiments are presented in Table 1. The volume–area distribution for each of the structures is given in Fig. 3. There is a large difference between the characteristics of the nickel-kieselguhr and the molybdena structures. Estimation of the distribution for the nickel pellet at higher pore radii is based on matching the area under the curve to the macropore void volume and assuming a symmetric distribution for radii greater than 200 Å

The variation of material properties is clearly demonstrated in Fig. 3. It is seen here that, although the densities of Pellets 1 and 2 are not greatly different, their respective pore-size distributions are not similar. The most probable radius of the nickel pellet is about 2500 Å, although this is an estimated value as described above, and that of the molybdena pellet about 360 Å. It is also clear that the molybdena pellets have much smaller diameter macropores than the supported nickel oxide pellet. The micropore region presents an entirely different situation; for the nickel pellet a large portion of total void volume is within the micropores while for the molybdena samples only a very small portion of total volume is contained in this

TABLE 1

PROPERTIES OF POROUS SOLIDS EMPLOYED IN DIFFUSION EXPERIMENTS

	Ni-0104-P	Mo-0401-P			Fe-0303-P
Pellet designation	1	2	3	4	—
Density (ρ, g/cc)	1.83	1.76	1.63	1.48	1.37
Total porosity (ϵ)	0.49	0.16	0.22	0.30	0.45
Macropore porosity (ϵ_a)	0.27	0.15	0.20	0.28	—
Most probable macropore radius (r, Å)	2800	340	355	380	—
Powder particle size (microns)	25	220	220	220	200
BET area (m^2/g)	86.1	28.3	28.3	28.3	—
Pellet thickness (L, cm)	1.20	1.02	0.91	1.13	1.20
Pressing force (lbs)	6000	6000	9000	12 000	5000
Pellet surface area (cm^2)	5.07	5.07	5.07	5.07	5.07

region. For the molybdena increasing density increases the dispersion to the left of the distribution curve, leaving the average radius relatively unaffected. This behavior differs from that reported for other structures (*5*, *15*), where the most probable macropore radius decreases with increasing density. In all cases here the change in density is reflected only in the macropore distribution; micropores are unaffected. In Fig. 4 are given local density values for the iron and nickel oxide samples (*16*). Results for the iron sample indicate density variation produced by the pelleting procedure for a relatively soft material, with little elastic relaxation after compression, and so should approximate the maximum anisotropy to be expected. The density of this sample is uniform in the radial direction, but deviations on the order of $\pm 10\%$ of the overall 1.37 g/cm³ are evident in the axial direction. These deviations are about the same as the accuracy of measurement, but the extensive data of Satterfield and Saraf (*17*) leave little doubt as to the possibility of such gradients. For the supported nickel sample, somewhat harder than the powdered metal, axial deviations from overall density are less than for iron—a bit larger than $\pm 5\%$. Since little radial variation of density was

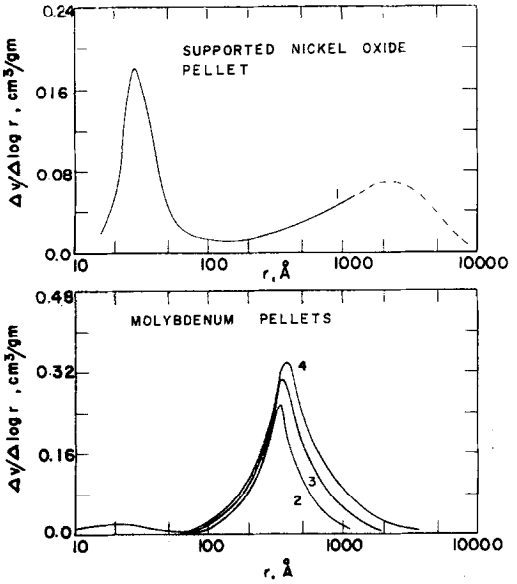

FIG. 3. Volume–area distributions for experimental porous structures.

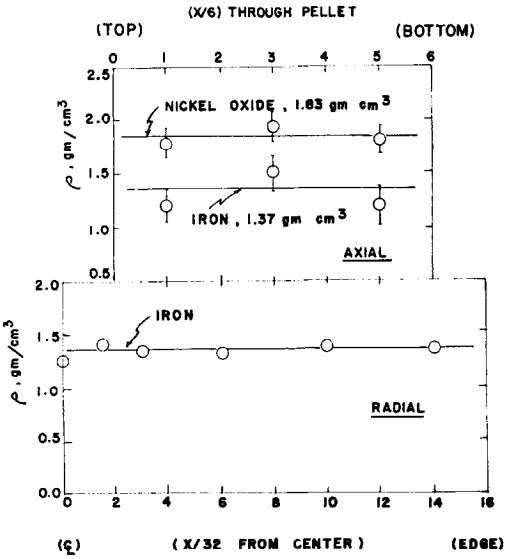

FIG. 4. Density homogeniety of iron and nickel oxide samples. (CL means "line of centers.")

noted for the soft material, this was not measured for the nickel. On the basis of these results for two rather diverse materials, axial density homogeniety within ±10% of the overall value is indicated for the porous samples studied.

Diffusional Flux Observations

The experimentally measured values of the diffusion fluxes of argon and helium at various pressures and temperatures are given in Fig. 5 for the nickel-on-kieselguhr pellet and in Figs. 6, 7 and 8 for the three

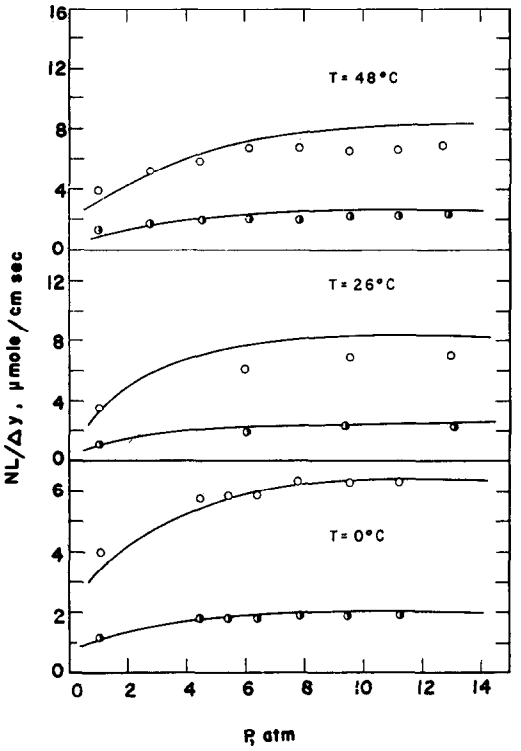

FIG. 5. Flux-pressure observations for nickel oxide on kieselguhr, Pellet 1. Open points represent helium flux, half-closed points argon flux. Solid lines computed from pore structure model.

different molybdena samples. Table 2 presents the corresponding flux ratio observations for all the porous pellets tested with the argon-helium system. It is seen that these observations are in agreement with the reciprocal square root of molecular weight dependence given by theoretical considerations for counterdiffusion of

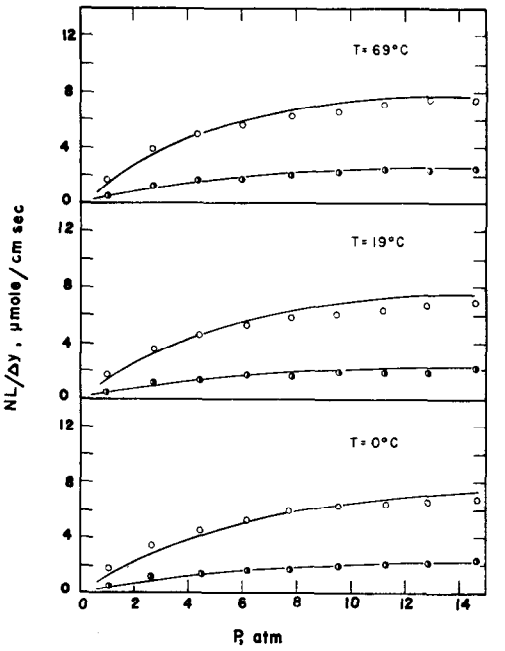

FIG. 6. Flux-pressure observations for molybdena, Pellet 2. Legend as in Fig. 5.

nonadsorbed gases in transition capillaries. The average of all observations, 3.04 ± 0.13, includes the theoretical value of 3.16

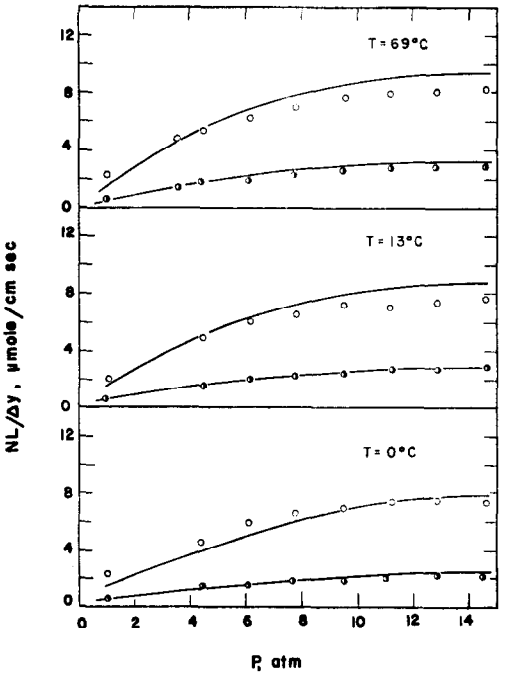

FIG. 7. Flux-pressure observations for molybdena, Pellet 3. Legend as in Fig. 5.

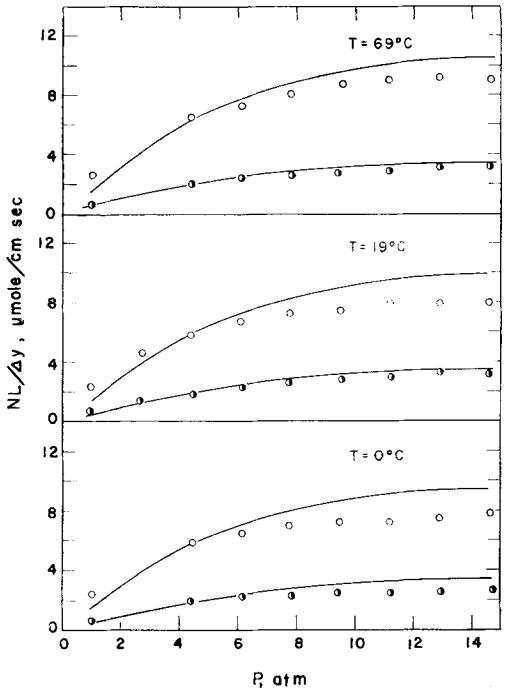

FIG. 8. Flux–pressure observations for molybdena, Pellet 4. Legend as in Fig. 5.

within the range of experimental error on flux ratio. Individual flux measurements are subject to experimental error of approximately ±5%, due mostly to concentration measurement error (*14*). Typical gas compositions and diffusion flow rates for a series of runs are given in Table 3.

A main objective of this study was to determine the effects of pressure and temperature on the diffusion fluxes. From the nature of the governing transport processes it can be shown at low pressures that the diffusion flux should be a linear function of the pressure, and at high pressures independent of pressure. This behavior is clearly demonstrated in Figs. 5–8. The slope of the pressure–flux curve in the low-pressure region is interesting. If it is

TABLE 3
TYPICAL GAS COMPOSITIONS AND DIFFUSION FLOW VALUES, PELLET 1 AT 48°C

Pressure (atm)	Mole % He in Ar	Mole % Ar in He	Ar Diffusion[a] (cc/min)	He Diffusion[a] (cc/min)
1.00	1.68	0.50	6.7	23.1
2.70	2.17	0.61	9.9	30.3
4.40	2.56	0.66	10.9	34.4
6.10	2.76	0.72	11.5	38.5
7.80	2.96	0.78	11.9	39.5
9.50	3.14	0.89	12.2	38.0
11.20	3.62	1.05	12.7	37.8
12.90	4.73	1.42	13.6	38.0

[a] Measured at 760 mm Hg and 22.0°C.

TABLE 2
HELIUM–ARGON FLUX RATIO DATA

Pellet	Temp. (°C)	Pressure (atm) 1.00	2.70	4.40	6.10	7.80	9.50	11.20	12.90	14.60
1	0	3.62	—	3.09	3.17[b]	—	3.30	3.20	—	—
1	26	3.14	3.17	—	3.18[c]	3.18	2.74	2.80	2.71	3.00
1	48	3.16	3.04	3.14	3.34	3.27	3.14	3.97	2.79	—
1	69	3.31	2.90	3.25	3.14	3.06	3.08	3.08	—	—
2	0	3.24	2.83	3.14	3.07	3.16	3.14	3.21	2.90	2.82
2	19	3.18	3.05	3.17	3.14	3.28	3.07	3.23	3.38	3.19
2	69	2.84	3.33	3.01	3.24	3.08	2.94	3.02	3.02	2.75
3	0	3.28	—	—	—	3.54	3.64	3.50	2.96	3.08
3	13	3.04	—	3.00	2.80	2.86	2.96	2.84	2.78	2.70
3	69	3.06	3.08[a]	2.98	3.19	2.98	2.96	2.89	2.80	2.60
4	0	3.02	—	3.06	2.85	2.87	2.91	2.83	2.81	2.75
4	19	3.19	—	3.43	3.29	2.96	2.80	2.68	2.64	2.56
4	69	3.04	—	3.14	2.93	3.04	3.06	2.96	2.90	2.86

Average of 102 observations = 3.04 ± 0.13

[a] P = 3.04 atm.
[b] P = 5.42 atm.
[c] P = 6.44 atm.

assumed that transport in the porous structure proceeds wholly by the Knudsen diffusion mechanism as the pressure, P, approaches zero, it can be seen from the form of the Knudsen diffusion equation that the initial slope of the flux–pressure curve is given by

$$\frac{d(N_A L/\Delta y)}{dP} = \frac{2r\bar{v}[y(L) - y(0)]}{3RTL} \quad (4)$$

In Eq. (4) the diffusion coefficient for the Knudsen region is defined by

$$D_K = \tfrac{2}{3}r\bar{v}$$

where r is the capillary radius and $\bar{v}$ the average molecular velocity. The right-hand term of Eq. (4) is not a function of the properties of the porous material, therefore the initial slope is directly proportional to r for any given structure. Examining the data of Fig. 5 for the nickel pellet, it is seen that a limiting value for this derivative is approximately 1.1 μmole/cm-atm sec while the initial slopes in Figs. 6–8 are the same at about 0.6 μmole/cm-atm sec. This is consistent with the most probable radius of each pellet, that of the supported nickel oxide being larger than that of the molybdena and the radii of the latter three samples being approximately equal. The solid lines drawn on these figures represent the diffusional flux values computed from the pore structure model; argon flux is calculated directly and helium flux determined from this value and the theoretical flux ratio, 3.16, for diffusion in the absence of surface migration. Detailed discussion of this fit is given in Part II (following paper).

An example of the temperature dependence of diffusion flux is given in Fig. 9 for the argon measurements on the four samples at the extreme of the pressures studied experimentally. The solid lines again are those computed from the pore structure model. It is interesting to note the change in shape of the curves from the low-pressure isobars to the high-pressure isobars. In all cases the low-pressure isobars exhibit only slight, if any, temperature dependence, while high-pressure isobars are definite functions of temperature. This result follows from the mixed nature of diffusional transport, as expressed in Eq. (1), which is occurring in the capillaries of the porous structure. In pores of very small diameter where Knudsen diffusion predominates the flux is inversely

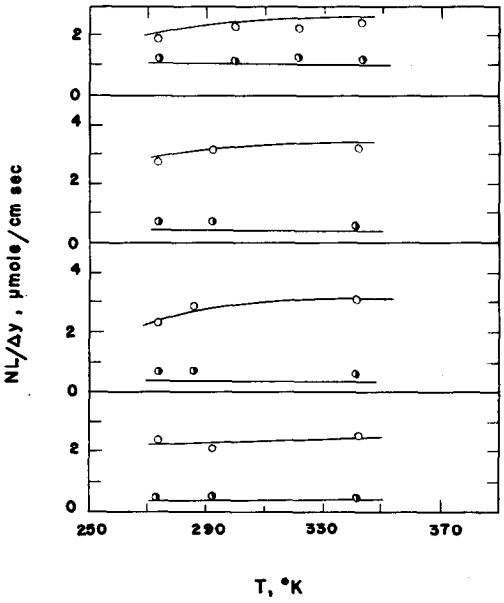

FIG. 9. Temperature dependence of argon diffusion flux. Open points are at 14.6 atm, half-closed points at 1 atm. Results presented in ascending order for Pellets 2, 3, 4, and 1. Solid lines computed from model.

proportional to $T^{1/2}$ at constant pressure, whereas in large capillaries where bulk diffusion predominates, flux is directly proportional to $T^{1/2}$. Thus, in a capillary of intermediate size the flux will be independent of the temperature at some "inversion" pressure. For a capillary of radius r and length L, the integrated form of Eq. (1) is

$$N_A = \frac{cD_{AB}}{L\alpha} \ln \left\{ \frac{[1 - \alpha y(L)] + \gamma}{[1 - \alpha y(0)] + \gamma} \right\} \quad (6)$$

D_{AB} is calculated from the Chapman-Enskog formula and can be represented by

$$D_{AB} = (A/P)T^{3/2} \quad (7)$$

where A is some function of molecular parameters. The Knudsen coefficient writ-

ten in equivalent form from Eq. (5) is

$$D_K = ET^{1/2} \tag{8}$$

where E is a constant defined in terms of capillary radius and molecular weight. Then

$$\gamma = (A/E)(T/P) \equiv D(T/P) \tag{9}$$

Substituting these explicit temperature dependences into Eq. (6) and taking the derivative of flux with respect to temperature at constant pressure, we have for $(dN_A/dT) = 0$

$$\frac{1}{G_2 + D(T/P)} - \frac{1}{G_1 + D(T/P)} = \ln\left[\frac{G_1 + D(T/P)}{G_2 + D(T/P)}\right] \tag{10}$$

where G_1 is $[1 - \alpha y(0)]$ and G_2 is $[1 - \alpha y(L)]$. For the conditions employed in a Wicke-Kallenbach experiment $y(0) \to 1$ and $y(L) \to 0$, so $G_1 = (1 - \alpha)$ and $G_2 = 1$. For these conditions, Eq. (10) becomes

$$2\left(\frac{DT}{P}\right) \times \left[\frac{\alpha}{(1-\alpha) + (2-\alpha)(DT/P) + (DT/P)^2}\right] = \ln\left[\frac{1 + (DT/P)}{(1-\alpha) + (DT/P)}\right] \tag{11}$$

The relationship between (DT/P) and α is plotted in Fig. 10. From this figure a value of (DT/P) is determined from the known α for the system. The constant D may be evaluated from Eqs. (7) and (8), and P is computed from the known T of the system. This P is the pressure at which the value of (dN_A/dT) is zero; that is, the diffusion flux changes from a square-root temperature dependence to a reciprocal square-root temperature dependence at this inversion pressure.

For an α of (—2.16), which corresponds to the helium-argon system, and a most probable radius of 350 Å, which corresponds to the molybdena samples used in the experiments, D is calculated to be 3.3×10^{-2} atm/°K, and at 300°K the inversion pressure is 5.3 atm. This value, based on average radius, is in general agreement with measured values for the experimental structures, approximately 3 atm. The inversion pressure is actually a function of temperature, but the relationship is so slight that for a given diffusing pair the value of this function is essentially dependent only on capillary dimension. For the helium-argon system in a porous structure of most probable radius 350 Å, a change in temperature from 50° to 100°C changes the value of inversion pressure by less than 10%.

An example of the effect of porosity on the diffusion flux is given in Fig. 11 for the molybdena samples for the extremes of the pressures employed in the experimental work. The result, a nearly linear relationship between flux and porosity, is very interesting. While the data reported are quite specific and linearity in general would not be expected to prevail over a large range of porosity, it is apparent that reasonable estimates of diffusional variation for this system can be based on linear

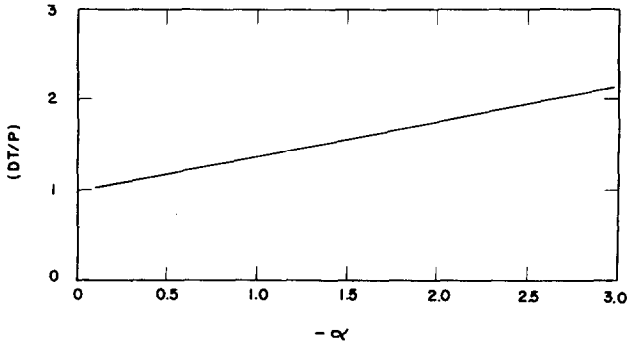

FIG. 10. Inversion pressure parameter as a function of α from Eq. (11).

extrapolation. The statistical model of pore structure (*5*), which involves the square of porosity in prediction of diffusional rates, is not in accord with these experimental results. One must be careful in interpretation here, since the representation of diffusional flux in terms of the porosity is an oversimplification; the

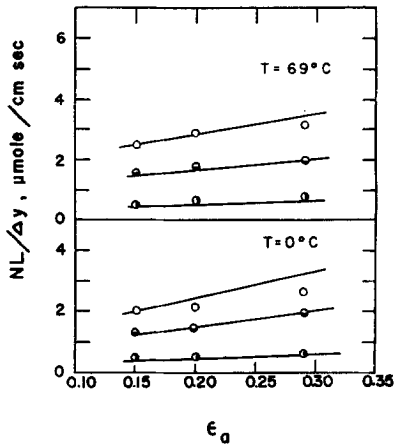

FIG. 11. Effect of porosity on argon diffusion flux for molybdena pellets: ○, 14.6 atm; ◒, 4.4 atm; ◑, 1 atm. Solid lines computed from pore structure model.

nickel oxide pellet, which has a much different volume–area distribution, does not fit the correlation of Fig. 11. In many cases, however, it does appear that the contribution of the micropore structure to transport effects is minor, if at all significant, and representation of pore structure in terms of macropore characteristics is sufficient.

CONCLUSIONS

The experimental study of argon–helium counterdiffusion in the porous structures investigated demonstrated that the flux ratios are, within experimental error, equal to those predicted by the theoretical relationships (*7*, *9*) and do not vary with pressure or temperature. This observation is in agreement with the conclusion on theoretical grounds given elsewhere (*10*) that flux ratio would not be expected to vary from the inverse square root of molecular weight relationship for normal ranges of temperature and pressure in porous structures such as those studied here. Agreement between experimental and theoretical flux ratios is also strong indirect evidence of the absence of surface adsorption and migration, since it has been shown (*14*) experimentally that surface transport alters flux ratios as well as flux magnitudes.

Diffusional transport rates increase with pressure at lower pressures, but become independent of pressure variation at high pressures. This is to be expected from the nature of the predominating bulk diffusion process which occurs at high pressures (molecular mean free paths become significantly smaller than capillary dimensions), which is independent of pressure. The existence of differing regions of temperature dependence of transport rate predicted by Eqs. (1) and (6) was verified experimentally by measurement of the inversion pressure, that pressure at which flux is independent of temperature, for the porous materials studied. The theory predicts an inversion pressure of 5.3 atm and a temperature dependence of flux approaching $T^{1/2}$ at pressures above this point for the molybdena samples, while experimental values are 3 atm and $T^{0.4}$, respectively. This is considered to be quite good agreement in view of the approximation involved in using the single capillary equation with average poprerties to represent the overall structure, and provides additional support to prior experimental indication (*5*, *8*) of the validity of Eq. (1) for description of diffusion in transition capillaries.

The effect of porous structure on rates of diffusional transport is seen experimentally to be approximately linear in porosity for the range of materials studied. The result cannot be expected, however, to be valid *a priori* for any material; the effects of porous structure must be treated in terms of some model representation of the structure and parameters associated with the model be evaluated in terms of measurable properties of the structure. This problem, as distinct from the correlation afforded here and previously (*11*), is discussed in Part II (following paper).

Acknowledgments

The authors are indebted to the National Science Foundation for support of this work, to Dr. A. B. Stiles of E. I. duPont Company for determining the macropore volume–area distributions, and to Harshaw Chemical Company for their gift of the porous materials.

References

1. Zeldowich, J. B., *Acta Physicochem.* **10**, 583 (1939).
2. Thiele, E. W., *Ind. Eng. Chem.* **31**, 916 (1939).
3. Satterfield, C. N., and Sherwood, T. K., "The Role of Diffusion in Catalysis." Addison-Wesley, Reading, Massachusetts, 1963.
4. Mingle, J. O., and Smith, J. M., *AIChE J.* **7**, 243 (1961).
5. Wakao, N., and Smith, J. M., *Chem. Eng. Sci.* **17**, 825 (1962).
6. Stewart, W. E., and Johnstone, M. F. L., *J. Catalysis* **4**, 248 (1965).
7. Evans, R. B., Watson, G. M., and Mason, E. A., *J. Chem. Phys.* **35**, 2076 (1961).
8. Scott, D. S., and Dullien, F. A. L., *AIChE J.* **8**, 113 (1962).
9. Hoogschagen, J., *Ind. Eng. Chem.* **47**, 906 (1955).
10. Butt, J. B., and Foster, R. N., *Nature* **211**, 284 (1966).
11. Foster, R. N., and Butt, J. B., *AIChE J.* **11**, 180 (1966).
12. Weisz, P. B., *Z. Physik. Chem.* (*Frankfurt*). **11**, 1 (1957).
13. Wicke, E., and Kallenbach, R. *Kolloid Z.* **97**, 135 (1941).
14. Foster, R. N., PhD Thesis, Yale Univ., New Haven, Connecticut, 1966.
15. Evans, R. B., Truitt, S., and Watson, G. M., *J. Chem. Eng. Data* **6**, 522 (1961).
16. Irving, J. P., PhD Thesis, Yale Univ., New Haven, Connecticut, 1966.
17. Satterfield, C. N., and Saraf, S. K., *Ind. Eng. Chem. Fundamentals* **4**, 451 (1965).